ACS APPLIED MATERIALS & INTERFACES

Research Article

www.acsami.org

Phosphonium-Organophosphate Ionic Liquids as Lubricant Additives: Effects of Cation Structure on Physicochemical and Tribological Characteristics

William C. Barnhill,[†] Jun Qu,*[,†] Huimin Luo,[‡] Harry M. Meyer, III,[†] Cheng Ma,[†] Miaofang Chi,[†] and Brian L. Papke[§]

[†]Materials Science and Technology Division, Oak Ridge National Laboratory, P.O. Box 2008, MS-6063, Oak Ridge, Tennessee 37831-6063, United States

[‡]Energy and Transportation Science Division, Oak Ridge National Laboratory, Oak Ridge, Tennessee 37831, United States

[§]Shell Technology Center Houston, Shell Projects and Technology (US), 3333 Hwy 6 South, Houston, Texas 77210-3101, United States

ABSTRACT: Our previous work suggested great potential for a phosphonium-organophosphate ionic liquid (IL) as an antiwear lubricant additive. In this study, a set of five ILs were carefully designed and synthesized, with identical organophosphate anions but dissimilar phosphonium cations, to allow systematic investigation of the effects of cation alkyl chain length and symmetry on physicochemical and tribological properties. Symmetric cations with shorter alkyl chains seem to increase the density and thermal stability due to closer packing. On the other hand, either higher cation symmetry or longer alkyl moieties induce a higher viscosity, though the viscosity index is dependent more on molecular mass than on symmetry. While a larger cation size generally increases an IL's solubility in nonpolar hydrocarbon oils, six-carbon seems to be the critical minimum alkyl chain length for high oil miscibility. Both the two ILs, that are mutually oil miscible, have demonstrated promising lubricating performance at 1.04% treat rate, though the symmetric-cation IL moderately outperformed the asymmetric-cation IL. Characterizations on the tribofilm formed by the best-performing symmetric-cation IL revealed the film thickness, nanostructure, and chemical composition. Results here provide fundamental insights for future molecular design in developing oil-soluble ILs as lubricant additives.

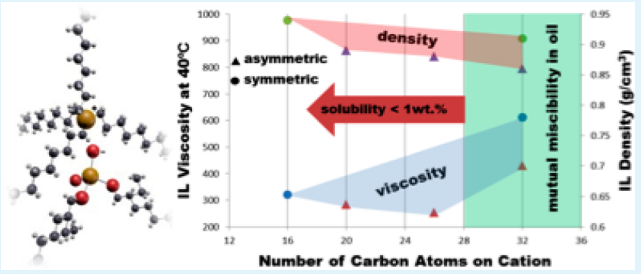

KEYWORDS: *ionic liquid, gas-to-liquid oil, lubricant antiwear additive, phosphonium, organophosphate, oil solubility*

1. INTRODUCTION

With over a billion registered vehicles in the world, there exists a clear benefit to increasing internal combustion (IC) engine efficiency and longevity. IC engines extract power from a piston and cylinder assembly in a way that necessitates prolonged sliding interaction between surfaces. Engine lubricants are required to mediate the contact pressure between engine bearing interfaces, such as piston rings against cylinder liners, to minimize wear and friction. More than 10% of the energy produced by combustion is dissipated by hydrodynamic drag induced by shearing the lubricant film at the bearing interfaces.[1] Although this loss cannot be totally eliminated, minimizing it via advanced lubricants can result in significant energy savings.

When relative motion exists between two adjacent lubricated surfaces, the interaction can be categorized as being in boundary, mixed, elastohydrodynamic, or hydrodynamic lubrication. A piston in an IC engine is constrained to reciprocating, linear motion; therefore, it must cease movement before reversing direction. The regions in which this reversal occurs are under boundary lubrication conditions and are prone to wear due to more frequent asperity contacts. Higher viscosity engine oils generate a thicker lubricant film at the interface, and generally provide better wear protection near top and bottom dead centers of the stroke. Conversely, the piston−cylinder interface is within the elastohydrodynamic and hydrodynamic regimes for the majority of a stroke. There is virtually no wear in these regimes; thus, it is desirable to use lower viscosity oils to reduce irreversibilities associated with elastohydrodynamic drag to increase energy efficiency. These conflicting ideas can be reconciled through implementation of more effective additive packages that allow the use of lower viscosity oil while retaining antiwear functionality.

Ionic liquids (ILs) have been utilized in a diverse array of applications over the past half-century with majority use as "customizable" solvents or electrolytes. Generally, ILs possess low volatility, low combustibility, and high thermal stability. Since 2001, research interest in ILs has expanded into lubrication.[2] Early work was centered on ILs containing

Received: September 29, 2014
Accepted: November 17, 2014
Published: November 17, 2014

   dx.doi.org/10.1021/am506702u | ACS Appl. Mater. Interfaces 2014, 6, 22585−22593

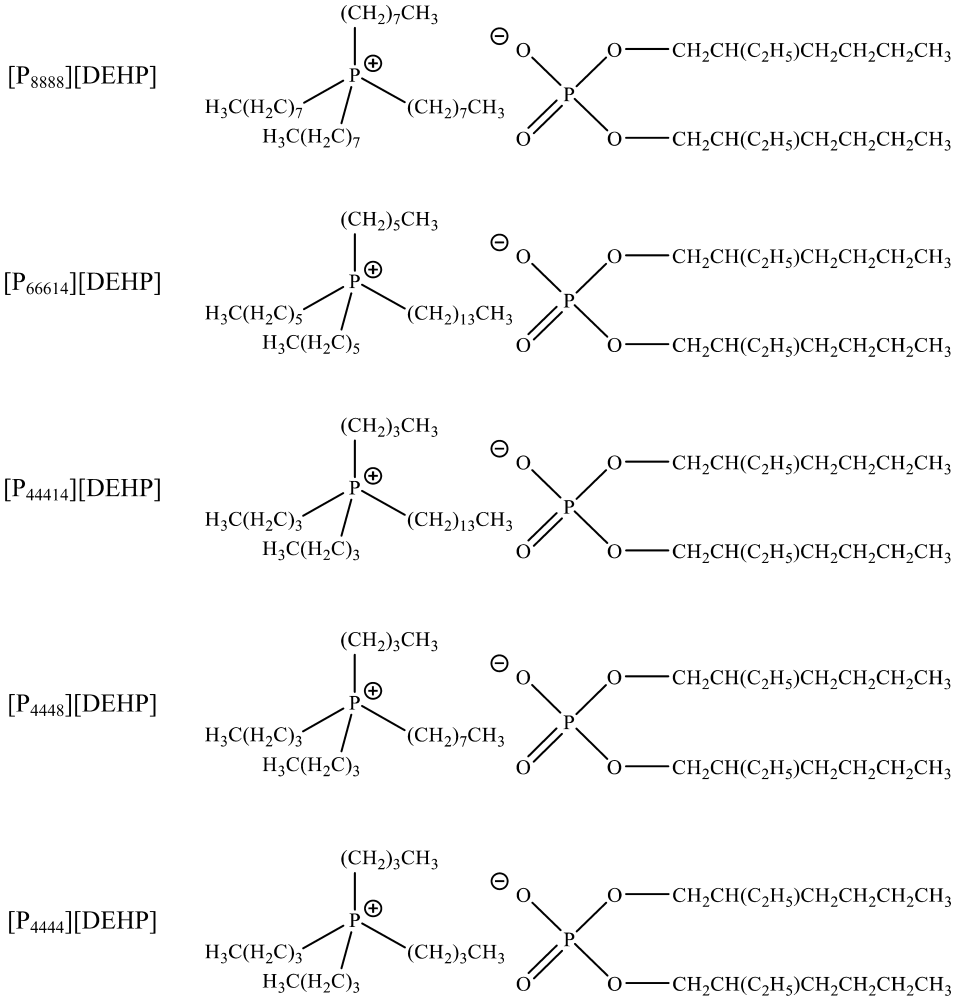

Figure 1. Molecular structures of selected phosphonium-organophosphate ILs.

Table 1. Molecular Weight, Oil-Solubility, Density, and Viscosity of Selected ILs

			viscosity of neat IL (cP)				
ionic liquid	molecular weight	density (g/cm^3)	23 °C	40 °C	100 °C	viscosity index	solubility in GTL oil (wt %)
$[P_{8888}][DEHP]$	805.26	0.91	>1500[a]	611.8	68.2	188	>50
$[P_{66614}][DEHP]$	805.26	0.86	1045	429.0	49.5	177	>50
$[P_{44414}][DEHP]$	721.10	0.88	711.4	252.8	25.2	128	~1
$[P_{4448}][DEHP]$	636.94	0.89	788.6	282.9	30.5	147	<1
$[P_{4444}][DEHP]$	580.83	0.94	940.7	320.1	30.9	134	<1

[a]Above the upper limit of the measurement range.

imidazolium cations with various fluorine-containing anions.[3−7] Much work of using ILs as lubricant additives involved oil−IL emulsions or very low concentrations of ILs in base oils due to many ILs' inherent insolubility in nonpolar hydrocarbon oils.[8−15] Some applied polar base stocks to facilitate solubility.[16,17]

In 2012, we reported trihexyltetradecylphosphonium bis(2-ethylhexyl) phosphate ($[P_{66614}][DEHP]$) with mutually miscible properties in nonpolar hydrocarbon oils and promising antiwear characteristics as a lubricant additive for steel-cast iron contacts.[18−20] Later studies from a couple of other groups[21,22] reinforced the concept of using $[P_{66614}][DEHP]$ as an antiwear additive by confirming the oil miscibility and demonstrating effective wear protection in lubricating steel−aluminum[21] and steel−steel[22] contacts. Several other phosphorus-containing ILs[19,21,22] have since been explored as lubricant additives, and the group of alkylphosphonium-organophosphate ILs demonstrated superior lubricating performance compared to a conventional antiwear additive[20] and other phosphorus-containing groups.[21] However, there is lack of fundamental understanding of the correlations between the ion structures and the IL's physicochemical and tribological properties.

In this study, we carefully designed and synthesized five alkylphosphonium-organophosphate ILs containing identical anions but different cations, including $[P_{66614}][DEHP]$ and four new ILs. Particularly, the two ILs containing symmetric cations are newly invented and patent pending.[25] Such a group of ILs allowed a systematic investigation of the effects of cation symmetry and alkyl chain length on the ILs' oil solubility, density, viscosity, thermal stability, corrosion behavior, and

Table 2. IL Treat Rates in the Base Oil and Viscosities of the Oil−IL Blends

lubricant	target IL conc (wt %)	P conc (wt %)	viscosity of GTL-IL blend (cP)		
			23 °C	40 °C	100 °C
GTL 4 cSt base oil	0	0	29.92	15.11	3.28
GTL 4 + $[P_{8888}][DEHP]$	1.04	0.08	29.97	15.08	3.25
GTL 4 + $[P_{66614}][DEHP]$	1.04	0.08	30.02	15.04	3.26
GTL 4 + $[P_{44414}][DEHP]$	0.93	0.08	30.13	15.14	3.27
GTL 4 + $[P_{4448}][DEHP]$	0.82	0.08	not measured	not measured	not measured
GTL 4 + $[P_{4444}][DEHP]$	0.75	0.08	30.04	15.06	3.27

lubricating properties. While most of the literature paid more attention to the anion chemistry,[19,21−24] results here clearly suggest that the cation structure plays an important role as well.

2. EXPERIMENTAL DETAILS AND MATERIALS

2.1. Synthesis. Five quaternary phosphonium-organophosphate ionic liquids with different cation structures but the same anion structure were investigated in this study. They are tetraoctylphosphonium bis(2-ethylhexyl) phosphate ($[P_{8888}][DEHP]$), $[P_{66614}][DEHP]$, tributyltetradecylphosphonium bis(2-ethylhexyl) phosphate ($[P_{44414}][DEHP]$), tributyloctylphosphonium bis(2-ethylhexyl)-phosphate ($[P_{4448}][DEHP]$), and tetrabutylphosphonium bis(2-ethylhexyl) phosphate ($[P_{4444}][DEHP]$). The ionic structures of these ILs are shown in Figure 1, and their physical properties are listed in Table 1.

The synthesis of $[P_{66614}][DEHP]$ had been reported in our earlier work,[18] and $[P_{4444}][DEHP]$ was kindly provided by Cytec Industries Inc., Niagara Falls, ON, Canada. The purity of $[P_{66614}][DEHP]$ and $[P_{4444}][DEHP]$ was determined using titration at Cytec to be 98% and 97%, respectively.

$[P_{8888}][DEHP]$, $[P_{44414}][DEHP]$, and $[P_{4448}][DEHP]$ were newly synthesized and characterized at ORNL, and the detailed procedures are described as follows. Proton nuclear magnetic resonance (NMR) analysis was carried out using a Bruker MSL-400 at 400 MHz. Spectra were obtained in $CDCl_3$ with reference to TMS (0 ppm) for ^1H.

Details for $[P_{8888}][DEHP]$ follow: Tetraoctylphosphonium bromide {$[P_{8888}]Br$, 40.58 g, 72.0 mmol} and bis(2-ethylhexyl)phosphoric acid (HDEHP, 23.2 g, 72.0 mmol) were mixed in 90 mL of deionized water (DI H_2O, 18.2 MΩ cm) and 100 mL of hexanes. To this stirred suspension was added a solution of sodium hydroxide (NaOH, 2.88 g, 72.0 mmol) in 75 mL of DI H_2O dropwise at room temperature. The white suspension became clear after the addition of NaOH was completed. The mixture continued to be stirred at room temperature overnight.The upper organic phase was separated and washed with DI H_2O four times to ensure removal of NaBr. Solvents were distilled off by rotary evaporator, and the product was dried at 70 °C under vacuum for 4 h to yield $[P_{8888}][DEHP]$ as a viscous liquid (57.0 g, 70.8 mmol, yield: 93.8%). The water content of $[P_{8888}][DEHP]$ was 0.1%. Proton nuclear magnetic resonance (^1H NMR, $CDCl_3$, ppm): 0.85−0.87 (m, 24H, $8CH_3$), 1.27−1.36 (m, 56H, $28CH_2$), 1.44 (m, 2H, 2CH), 1.67 (m, 8H, $4CH_2$), 3.31 (m, 8H, $4NCH_2$), 3.80 (m, 4H, $2OCH_2$). ^{13}C NMR ($CDCl_3$, ppm): 10.81 ($2CH_3$), 13.96 ($4CH_3$), 14.02 ($2CH_3$), 22.02 ($4CH_2$), 22.52 ($4CH_2$), 23.04 ($2CH_2$), 23.09 ($4CH_2$), 26.28 ($4CH_2$), 28.92 ($2CH_2$), 29.06 ($4CH_2$), 29.87 ($4CH_2$), 31.64 ($4CH_2$), 40.09 (2CH), 58.84 ($4NCH_2$), 67.82 ($2OCH_2$).

Details for $[P_{44414}][DEHP]$ follow: Tributyltetradecylphosphonium chloride {$[P_{44414}]Cl$, 36.47 g, ∼49% in aqueous solution, 41.1 mmol} and bis(2-ethylhexyl)phosphoric acid (HDEHP, 13.26 g, 41.1 mmol) were mixed in 58 mL of hexanes. To this stirred mixture was added a solution of sodium hydroxide (NaOH, 1.64 g, 41.1 mmol) in 45 mL of DI H_2O (18.2 MΩ cm) dropwise at room temperature. The mixture continued to be stirred at room temperature overnight. The upper organic phase was separated and washed with DI H_2O four times to ensure removal of NaCl. Solvents were distilled off by rotary evaporator, and the product was dried at 70 °C under vacuum for 4 h to yield $[P_{44414}][DEHP]$ as a viscous liquid (29.1 g, 40.4 mmol, yield: 98.3%). The water content of $[P_{44414}][DEHP]$ was 0.3%. ^1H NMR ($CDCl_3$, ppm): 0.85−0.90 (m, 24H, CH_3), 1.24−1.31 (m, 36H, CH_2), 1.50−1.55 (m, 18H CH_2 and CH), 2.45 (m, 8H, PCH_2), 3.72 (m, 4H, OCH_2). ^{13}C NMR ($CDCl_3$, ppm): 10.94 (CH_3), 13.48 (CH_3), 14.09 (CH_3), 18.44 (CH_3), 18.91 (CH_3), 21.91 (CH_2), 22.61 (CH_2), 23.13 (CH_2), 23.31 (CH_2), 23.88 (CH), 29.04 (CH_2), 29.27 (CH_2), 29.56 (CH_2), 30.11 (CH_2), 31.63 (CH_2), 40.45 (CH_2), 67.30 ($2CH_2$)

Details for $[P_{4448}][DEHP]$ follow: Tributyloctylphosphonium chloride {$[P_{4448}]Cl$, 10.96 g, 31.3 mmol} and bis(2-ethylhexyl)-phosphoric acid (HDEHP, 10.08 g, 31.3 mmol) were mixed in 40 mL of hexanes. To this stirred mixture was added a solution of sodium hydroxide (NaOH, 1.25 g, 31.3 mmol) in 30 mL of DI H_2O (18.2 MΩ cm) dropwise at room temperature. The mixture continued to be stirred at room temperature overnight. The upper organic phase was separated and washed with DI H_2O four times to ensure removal of NaCl. Solvents were distilled off by rotary evaporator, and the product was dried at 70 °C under vacuum for 4 h to yield $[P_{4448}][DEHP]$ as a viscous liquid (17.68 g, 27.8 mmol, yield: 88.8%). The water content of $[P_{4448}][DEHP]$ was 0.3%. ^1H NMR ($CDCl_3$, ppm): 0.85−1.00 (m, 24H, CH_3), 1.28−1.40 (m, 24H, CH_2), 1.49−1.54 (m, 18H CH_2 and CH), 2.42 (m, 8H, PCH_2), 3.74 (m, 4H, OCH_2). ^{13}C NMR ($CDCl_3$, ppm): 10.90 (CH_3), 13.44 (CH_3), 14.05 (CH_3), 18.40 (CH_3), 18.67 (CH_3), 21.65 (CH_2), 22.50 (CH_2), 23.09 (CH_2), 23.27 (CH_2), 23.85 (CH), 28.91 (CH_2), 29.01 (CH_2), 30.06 (CH_2), 31.62 (CH_2), 40.40 (CH_2), 67.39 ($2CH_2$)

A low viscosity gas-to-liquid 4 cSt (GTL 4) base oil was provided by Shell Global Solutions (TX) and used as the base stock in this research. The GTL oil was synthesized via the Fischer−Tropsch process that produces alkanes from carbon monoxide and hydrogen obtained from natural gas.

All ILs in this work contain phosphorus. International Lubricants Standardization and Approval Committee (ILSAC) GF-5 specifications limit phosphorus content in engine oils to 800 ppm. Guided by this restriction, the five ILs were blended with GTL 4 to the maximum allowable phosphorus content resulting in treat rates of 0.75−1.04 wt %, as shown in Table 2.

2.2. Characterization. Each IL's oil solubility was determined by incrementally decreasing combinations of IL and GTL 4 from a 1:1 ratio until solubility was reached. The solute and solvent were mixed and vigorously shaken for 1 min. The samples were then placed in a centrifuge for 3 min at 13 000 rpm. The oil−IL blends were examined under bright lighting for evidence of separation or cloudiness right after centrifuge and 24 h after.

Thermogravimetric analysis (TGA) was performed on the ILs in air (allowing oxidation) using a TA Instruments (DE) TGA-2950 at a 10 °C per minute heating rate.

Viscosities of the neat ILs and oil-IL blends at 23, 40, and 100 °C were measured using a Petrolab (OK) MINIVIS II viscometer (falling ball technique). At least four measurements were conducted for each fluid to ensure a standard deviation less than 1%.

2.3. Corrosion and Tribological Testing and Analysis. Open-air corrosion testing was performed by placing a drop of each candidate IL directly onto a 25.4 × 25.4 mm^2 CL35 cast iron surface in an ambient environment for 7 days. Evaporation was not a concern due to ILs' low volatility. Electrochemical corrosion tests were carried out on the two oil-miscible ILs, $[P_{8888}][DEHP]$ and $[P_{66614}][DEHP]$, at room temperature, using the potentiodynamic polarization technique with a three-electrode electrochemical cell. A disk of cast

iron with 1 cm^2 exposed area was used as the working electrode, which was immersed in the electrolyte for 15 min before starting the experiment. A 20 mL portion of the IL to be tested served as the electrolyte. A Pt wire was used as the counter electrode, and Ag/AgCl (4 M KCl internal solution) was the reference electrode. The sample was polarized at potentials from −1.0 to +1.50 V versus open circuit potential at a scanning rate of 0.166 mV/s under aerated conditions. All electrochemical tests were conducted in the ambient environment using a potentiostat model CHI 700C (CH Instruments, Inc., Austin, TX).

Tribological wear and friction testing was performed on a Phoenix Tribology Ltd. (Hampshire, U.K.) Plint TE77 reciprocating sliding tribometer. A ball-on-flat geometry was chosen using an AISI 52100 steel ball against a CL35 (Metal Samples Company, AL) gray cast iron flat. The cast iron flats were first polished using 600 grit silicon carbide grinding paper producing a lay perpendicular to the sliding direction. All interacting surfaces were cleaned with isopropyl alcohol and air-dried before testing. The Plint TE77 obtains friction data *in situ* by taking tangential force measurements using a piezoelectric load cell. All lubricant blends were well-shaken before use. Testing for all specimens was carried out at 100 °C under a normal load of 100 N for a total sliding distance of 1000 m. The ball reciprocated at 10 Hz with a stroke of 10 mm against the flat. At least three replicate tests were performed for each IL−oil blend and the base oil to assess repeatability. After tribological testing, balls and flats were cleaned with acetone and then isopropyl alcohol. Wear volumes were measured using a Veeco (now Bruker, TX) Wyko NT9100 white light interferometer.

A Hitachi S-4800 (Tokyo, Japan) scanning electron microscope (SEM) equipped with an EDAX SDD energy-dispersive spectroscopy (EDS) system was used to analyze the worn surface from the top. Cross-sectional composition and nanostructure were examined using a Hitachi HF-3300 transmission electron microscope (TEM) (300 kV, 1.3 Å resolution) bundled with a Bruker solid-state EDS detector. TEM samples were prepared using a Hitachi NB5000 focused ion beam (FIB) system with a gallium ion source to extract a thin cross-section of the tribofilm of interest. A carbon film and then a tungsten layer were deposited onto the wear scar before the FIB process to protect the tribofilm. A Thermo Scientific (MA) K-Alpha X-ray photoelectron spectrometer (XPS) was used for chemical analysis of the selected tribofilm. The X-rays used were monochromatic Al Kα photons, and photoemitted electrons were analyzed with a hemispherical energy analyzer. Surface compositions were calculated by measuring peak areas of the primary core levels for all elements present and normalizing the peak areas using tabulated sensitivity factors. Composition-depth profiles were obtained under 1 kV ion beam energy at high a current setting.

3. RESULTS AND DISCUSSION

3.1. Physical and Chemical Properties. *3.1.1. Oil Solubility.* Due to the identical anion structure among the five ILs, changes in oil solubility are governed solely by the cation structures. We hypothesized that more carbon atoms in the alkyl groups on the cation would improve the oil solubility by (1) diluting the charge density thus decreasing ion coordination, and (2) increasing intermolecular London dispersion forces between lipophilic moieties of the cations with the base oil molecules. ILs with long alkyl chain cations may possess interesting physicochemical properties,[26] and the effects of the anion chemistry and alkyl structure and chain length on the IL's oil solubility had been discussed elsewhere.[19,21,23,24]

Table 1 and Figure 2a show the oil solubility for each candidate IL. $[P_{66614}][DEHP]$ and $[P_{8888}][DEHP]$ are mutually miscible (>50 wt %) in the GTL 4 cSt base oil. The remaining ILs have marked lower oil solubility: $[P_{44414}][DEHP]$, $[P_{4448}][DEHP]$, and $[P_{4444}][DEHP]$ showing solubility limits of ∼1, <1, and <1 wt %, respectively. Similar solubility was observed for the five ILs in a poly-α-olefin (PAO) 4 cSt base oil. The prevailing trend from this data strongly supports our hypothesis of longer alkyl chains improving oil solubility. The abrupt drop in oil solubility due to shorter alkyl chains either on the cation (from $[P_{66614}]$ to $[P_{44414}]$) or on the anion (from [DEHP] to dibutyl phosphate as observed in our previous study[19]) implies that six carbons could be the critical minimum alkyl chain length for phosphonium-organophosphate ILs to achieve high oil miscibility.

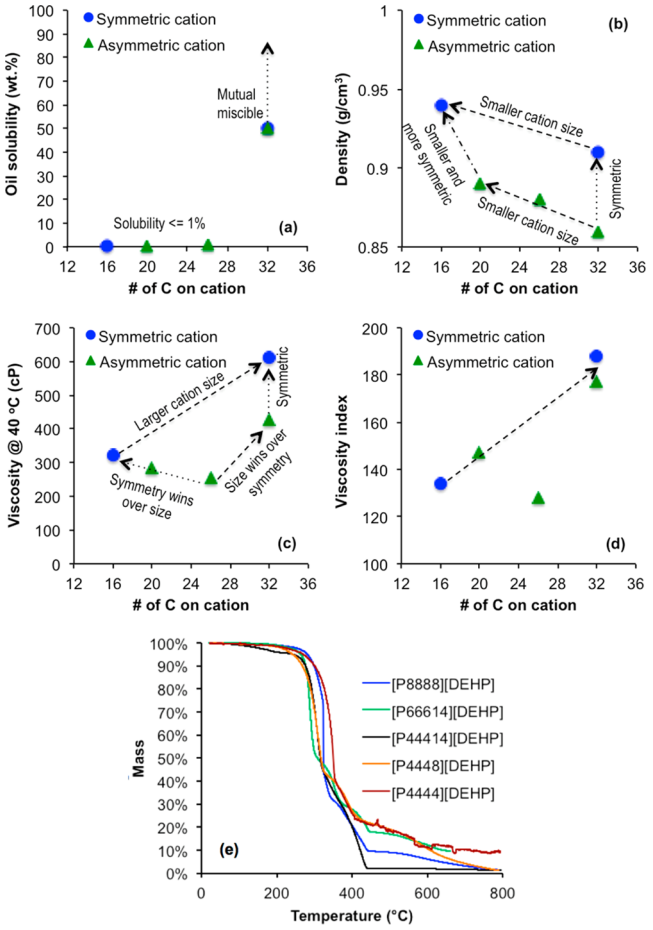

Figure 2. Effects of the cation structure on ILs' (a) oil-solubility, (b) density, (c) viscosity, (d) viscosity index, and (e) thermogravimetric behavior.

Table 2 lists the treat rates of ILs in the GTL 4 cSt base oil and the viscosities of the oil−IL blends. Evidently, the addition of ILs at such treat rates resulted in little change in viscosity.

3.1.2. Density, Viscosity, and Thermal Stability. Densities (ρ), viscosities, and viscosity indices of the five ILs are compared in Table 1 and Figure 2b−d. The ILs' densities are moderately affected by changes in cationic alkyl groups. As illustrated in Figure 2b, closer packing and thus higher density seems to be achieved by either reducing the size of the hydrocarbon chains, e.g., ρ ($[P_{4444}][DEHP]$) > ρ ($[P_{4448}][DEHP]$) > ρ ($[P_{44414}][DEHP]$) > ρ ($[P_{66614}][DEHP]$), or increasing the symmetry of the cation, e.g., ρ ($[P_{8888}][DEHP]$) > ρ ($[P_{66614}][DEHP]$).

The cationic alkyl groups' effect on viscosity (η) seems 2-fold: (1) more carbons per chain increase interionic interaction, (2) and higher symmetry causes closer packing and thus more interaction, as shown in Figure 2c. Both effects cause increased

resistance to shear flow and higher viscosity. For example, η ($[P_{66614}][DEHP]$) > η ($[P_{44414}][DEHP]$), η ($[P_{8888}][DEHP]$) > η ($[P_{4444}][DEHP]$), and η($[P_{8888}][DEHP]$) > η($[P_{66614}]$-$[DEHP]$). For $[P_{44414}][DEHP]$ versus $[P_{4448}][DEHP]$, the former has a slightly larger cation, but the latter has a slightly higher symmetry, and as a result of the competition between these two effects, the viscosities of these two ILs turn out to be similar. Evidently for $[P_{44414}][DEHP]$ versus $[P_{4444}][DEHP]$, the effect of cation symmetry was more significant.

The viscosity index (VI) is a measure of the variation in viscosity over an arbitrary temperature range. Reference temperatures of 40 and 100 °C are typically used in the automotive industry. Higher viscosity indices indicate more stable lubrication performance over this temperature range. Contrary to viscosity, the viscosity index generally seems to relate to IL mass but is little affected by the cation symmetry, as shown in Figure 2d. For instance, $[P_{8888}][DEHP]$ and $[P_{66614}][DEHP]$ both have identical mass and the highest mass of the five ILs but have different cation symmetry. These two ILs also possess higher viscosity indices than the other three ILs. Except that of $[P_{44414}][DEHP]$, the VIs of the remaining four ILs appeared to be proportional to their respective masses.

Figure 2e compares the TGA curves, and the on-site decomposition temperatures of all five ILs fall within a range 300−350 °C. The two ILs with symmetric cations ($[P_{4444}]$-$[DEHP]$ and $[P_{8888}][DEHP]$) showed slightly higher thermal stability than the rest three.

3.1.3. Corrosion Behavior. No evidence of pitting or other hints of corrosion were present on any of the cast iron surfaces that were exposed to the five ILs in open-air tests. Figure 3

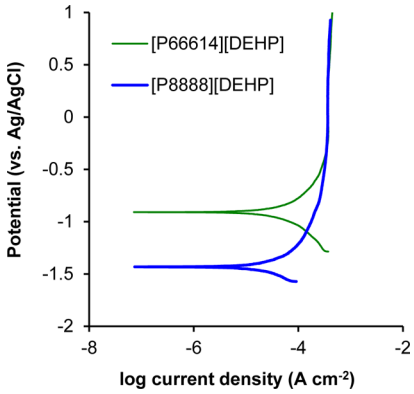

Figure 3. Potentiodynamic polarization curves of cast iron in the two oil-miscible ILs showing strong passivation.

shows the potentiodynamic polarization curves obtained for cast iron in neat $[P_{8888}][[DEHP]$ and $[P_{66614}][DEHP]$. Both showed classic active-passive behavior with strong passivation at a current density in the order of 10^{-4} A/cm^2. No corrosion damage or morphology change was observed on either of the iron surfaces electrochemically tested in the two ILs.

3.2. Friction and Wear Results. Because of the questionable oil solubility of $[P_{44414}][DEHP]$, $[P_{4448}][DEHP]$, and $[P_{4444}][DEHP]$ at the target concentrations (see Table 2), only $[P_{8888}][DEHP]$ and $[P_{66614}][DEHP]$, mutually miscible in the GTL 4 base oil, were selected for tribological testing and analysis.

Each friction trace in Figure 4 represents the average of three repeated tests. The baseline oil, GTL 4, exhibited a rapidly

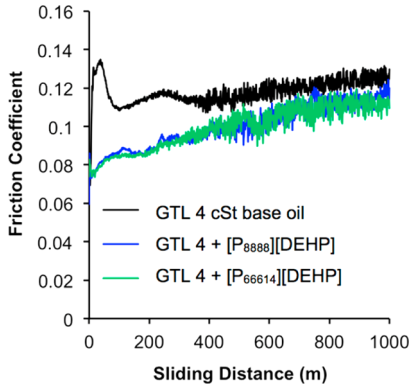

Figure 4. Friction coefficient traces of the base oil without and with IL additives.

increasing friction coefficient during the initial 25 m of sliding, an indication of scuffing.[27,28] Neither GTL 4 + 1.04% $[P_{8888}][DEHP]$ nor GTL 4 + 1.04% $[P_{66614}][DEHP]$ had such a rapid friction increase in the beginning of the tests. And, each blend reduced the average steady-state friction coefficient by ∼10% compared to GTL 4.

Addition of either $[P_{8888}][DEHP]$ or $[P_{66614}][DEHP]$ at the 1.04 wt % treat rate into the base oil significantly reduced the wear for the cast iron flat and steel ball (Table 3). Wear results here are an average of three replicates for each lubricant. Wear on the reciprocating steel ball specimens was consistently 2 orders of magnitude smaller than that on the cast iron flats. Two out of three repeats for GTL 4 without additive revealed scuffing and associated high wear, leading to a high standard deviation between tests. It is interesting to note the moderately better performance of GTL 4 + 1.04 wt % $[P_{8888}][DEHP]$ than that of GTL 4 + 1.04 wt % $[P_{66614}][DEHP]$ (Table 3). Phosphates have been used for years in lubricants and are known to be facilitators of protective tribofilm formation. Additionally, antiwear characteristics of ILs are thought to be more sensitive to changes in the anion. $[P_{8888}][DEHP]$ and $[P_{66614}][DEHP]$ share the identical organophosphate anion and have the same molecular weight, and differ only in their distribution of alkyl groups about the central phosphorus atom in their cations. Thus, the difference in wear performance may be attributed to the symmetry of the quaternary phosphonium cation. We hypothesize that the symmetric structured cation might allow better mobility for $[P_{8888}][DEHP]$ in the base oil to reach and interact with the surface asperities upon collisions to be more readily available in forming the protective tribofilm. Such hypothesis warrants further investigation.

3.3. Wear Scar Examination and Tribofilm Analysis. All wear scars were first examined using SEM for morphology imaging and using EDS for element detection. More comprehensive three-dimensional characterization[29] was then conducted on the tribofilm on the cast iron surface lubricated by GTL 4 + 1.04 wt % $[P_{8888}][DEHP]$. Aided by FIB, cross-sectional examination was carried out using TEM for film thickness measurement, using electron diffraction for phase identification, and using EDS for elemental mapping. XPS was used to analyze the tribofilm composition and ion sputtering allowed layer-by-layer analysis for revealing the composition variation of the tribofilm from top to bottom.

3.3.1. Top Surface SEM Morphology Examination and EDS Element Analysis. Representative SEM micrographs of the worn flat surface for each lubricant along with the

Table 3. Summary of Wear Results in the Base Oil without and without IL Additives

lubricant	flat wear volume (mm^3)	ball wear volume (mm^3)	total wear volume (mm^3)
GTL 4 cSt base oil	$1.12^{\pm 0.61}$	$0.51^{\pm 0.25} \times 10^{-2}$	$1.17^{\pm 0.61}$
GTL 4 + $[P_{8888}][DEHP]$	$0.10^{\pm 0.05}$	$0.10^{\pm 0.02} \times 10^{-2}$	$0.10^{\pm 0.05}$
GTL 4 + $[P_{66614}][DEHP]$	$0.18^{\pm 0.05}$	$0.09^{\pm 0.02} \times 10^{-2}$	$0.18^{\pm 0.05}$

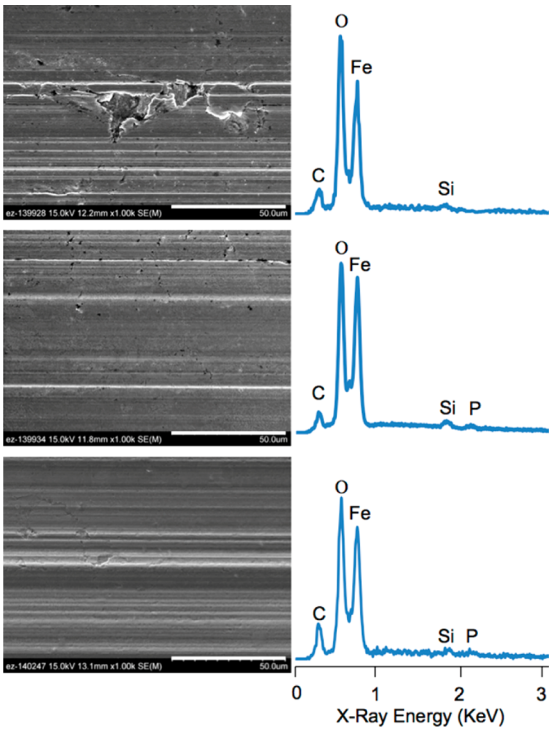

Figure 5. . SEM micrographs and EDS spectra. From top to bottom, wear scars lubricated by GTL 4 cSt base oil, GTL 4 + $[P_{8888}][DEHP]$, and GTL 4 + $[P_{66614}][DEHP]$. SEM micron bar: 50 μm.

corresponding EDS spectra are shown in Figure 5. The baseline lubricant (GTL 4) caused adhesive wear and plastic deformation as demonstrated by the deep grooves formed along the entire width and length of the scar. GTL 4 + 1.04% $[P_{66614}][DEHP]$ generated a smoother wear track with some shallower grooves. GTL 4 + 1.04% $[P_{8888}][DEHP]$ produced even less surface damage with the smoothest worn surface with fewest grooves in a more random pattern. The level of surface damage correlates well with the wear results described above.

In addition to the carbon, iron, and silicon peaks, EDS spectra in Figure 5 show prominent oxygen signal on the cast iron worn surfaces suggesting metal oxidation during the wear process. The wear tracks produced with the two oil−IL blends contain phosphorus as shown by the small peaks just above 2 keV, indicative of IL-induced tribofilms on the worn surfaces.

3.3.2. Cross-Sectional TEM Nanostructure Examination and EDS Elemental Mapping. Tribofilms formed by asymmetric-cation IL $[P_{66614}][DEHP]$ (blended in PAO 4 cSt base oil) on cast iron surfaces were previously examined.[18,20] In this study, the tribofilm examination was focused on the new symmetric-cation IL $[P_{8888}][DEHP]$ due to its superior wear protection (Table 3). Aided by FIB milling, cross-sectional TEM micrographs, EDS element mapping, and electron diffraction pattern of the tribofilm on the cast iron flat lubricated by GTL 4 + $[P_{8888}][DEHP]$ were obtained (Figure 6). This tribofilm appears to be single layered with a thickness varying from 10 to 200 nm. The diffraction pattern implies an amorphous matrix populated with nanocrystalline inclusions. The size of these inclusions is determined to be 1−10 nm by high magnification TEM imaging. EDS elemental maps show relatively uniform distribution of oxygen, iron, and phosphorus and discrete areas containing carbon (excluding the carbon signals across the top that are from FIB processing) throughout the thickness of the tribofilm. This tribofilm appears similar compared to that of the single-layer tribofilm from $[P_{66614}]$-$[DEHP]$ reported in ref 18 differing from the two-layer tribofilm observed in ref 20. Table 4 compares the tribofilm characteristics (based on cross-sectional TEM/EDS examination) between this work on $[P_{8888}][DEHP]$ and our previous studies on $[P_{66614}][DEHP]$.[18,20] Although mixed with different base oils, at different treat rates, against different sliders, and under different test conditions, the tribofilms formed on cast iron surfaces by these two ILs seem to have similar nanostructure and chemical composition. The only notable distinction is the double-layer structure (with a discrete oxide interlayer) observed in ref 20, which might be attributed to the combined higher load (240 N) and elevated temperature (100 °C) compared to ref 18 (160 N and 23 °C) and this work (100 N and 100 °C). Under the higher thermomechanical stresses in ref 20, more significant oxidation may occur on surface asperities in collision to grow pads of oxides during wear-in before sufficient IL ions decomposed to become available to form the IL tribofilm on top of the oxide layer.

3.3.3. Layer-by-Layer XPS Chemical Analysis. XPS core level spectra of key elements of the worn cast iron surface lubricated by GTL 4 + $[P_{8888}][DEHP]$ are shown in Figure 7. The red spectra represent binding energies for the initial 2−3 nm of the surface including the top of the tribofilm and any lubricant residue (even though all wear scars were carefully cleaned by solvents after wear testing). The green spectra were produced after 60 s of ion sputtering of the tribofilm to eliminate the surface contaminants.

As compared in the core level spectra, iron on the top surface of the tribofilm is primarily in the Fe^{3+} oxidation state (710.5 eV binding energy, BE) while Fe^{2+} (709.7 eV BE) becomes the major peak after 60 s sputtering. The ferric iron on the top surface is likely manifested as iron(III) oxide that developed during storage (several weeks) before XPS analysis. The phosphorus 2p spectra show a dominating P−O bond (133.7 eV BE) suggesting phosphates. The O 1s shows two distinct features: a peak at ∼531.5 eV BE is assigned to O−P bonding (excluding P−O−Fe), and another at 530.3 eV is attributed to O−Fe/P−O−Fe bonds. The higher amount of O−P detected on the top surface is possibly introduced by the IL residue, and the stronger O−Fe/P−O−Fe signal after 60 s of ion sputtering suggests most O atoms are bonded with iron phosphates and oxides. The same C 1s spectra (both before and after 60 s of sputtering) show a dominant peak at 285.0 eV BE assigned to C−C bonding. This indicates that the carbon content in the tribofilm might be from residue hydrocarbon chains on the partially decomposed organophosphate anions. The metallic Fe and carbide peaks after 60 s ion sputtering may be introduced by two sources: (1) iron substrate exposed by ion sputtering

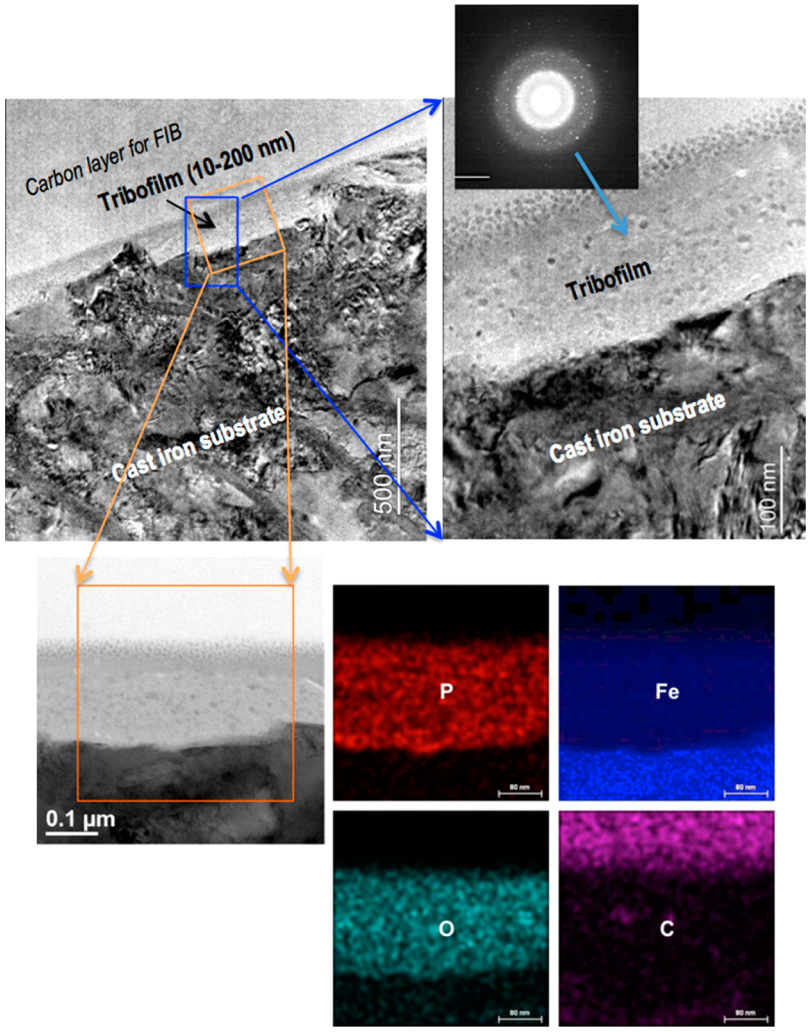

Figure 6. Cross-sectional TEM micrographs and electron diffraction pattern (top) and EDS elemental maps (bottom) of the tribofilm on the cast iron surface lubricated by GTL 4 + $[P_{8888}]$DEHP].

Table 4. Comparison of Tribofilms Formed by $[P_{8888}]$[DEHP] and $[P_{66614}]$[DEHP] Observed in Three Studies

	reciprocating sliding test (10 Hz oscillation with 10 mm stroke)			tribofilm (cross-sectional TEM/EDS)		
IL	base oil, IL treat rate	substrate (slider)	L, T, SD[a]	major elements	thickness (nm)	structure
$[P_{8888}]$[DEHP] (this study)	GTL 4 cSt, 1.04 wt %	cast iron (52100 steel ball)	100 N, 100 °C, 1000 m	Fe, O, P, C	10−200	single layer
$[P_{66614}]$[DEHP] (ref 18)	PAO 4 cSt, 5.0 wt %	cast iron (Mo-coated piston ring)	160 N, 23 °C, 1000 m	Fe, O, P, C	120−180	single layer
$[P_{66614}]$[DEHP] (ref 20)	PAO 4 cSt, 1.0 wt %	cast iron (Mo-coated piston ring)	240 N, 100 °C, 4320 m	Fe, O, P, C	60−220	double layer

[a]L, normal load; T, lubricant bulk temperature; SD, sliding distance.

and (2) iron wear debris within the tribofilm. On the basis of binding energy analyses, the tribofilm formed by $[P_{8888}]$-[DEHP], similar to that by $[P_{66614}]$[DEHP], is believed to be a composite of iron phosphates (or polyphosphates) and iron oxides.

The deconvoluted composition-depth profile (from 60 to 1790 s of ion sputtering) is shown in Figure 8a. As revealed in the cross-sectional TEM/EDS images in Figure 6, the thickness of the tribofilm varies (10−200 nm in a 2 μm-long TEM sample), and Fe, O, and P have relatively uniform distributions in the tribofilm from the top surface to the interface with the substrate. Therefore, the rising signals of metallic iron and carbide and dropping signals of tribofilm elements along the sputtering time are largely a consequence of substrate exposure from material removal during ion sputtering. Assuming minimal metallic iron and carbide is embedded in the tribofilm (both less than 1 at % on the surface survey scan), we removed these two substrate signals, renormalized other elements, and replotted the profile in Figure 8b. This mitigates the bias from the increasingly exposed substrate and better reflects the composition change through the thickness of the tribofilm. The ratios of O(O−P):P and O(O−Fe/P−O-Fe):Fe(ion) are relatively constant throughout the film thickness, though the oxygen contents are somewhat higher than expected. Results

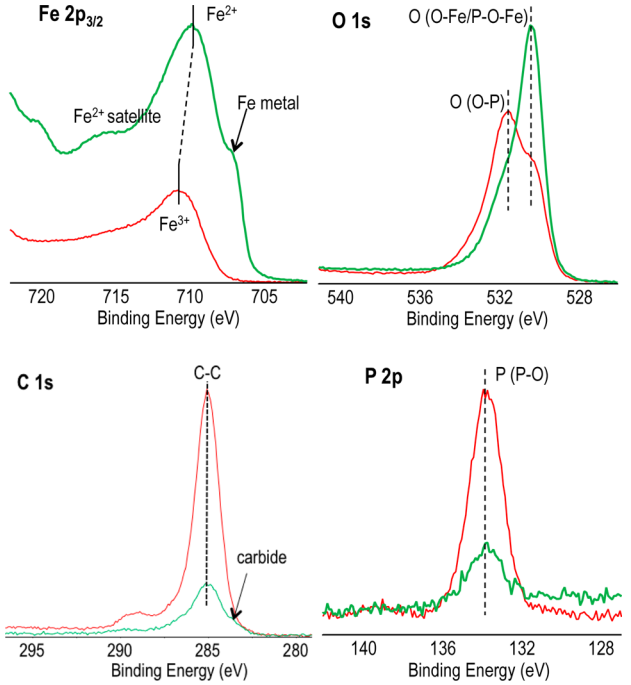

Figure 7. XPS core level spectra of key elements for the tribofilm on the cast iron surface lubricated by GTL 4 + $[P_{8888}][DEHP]$.

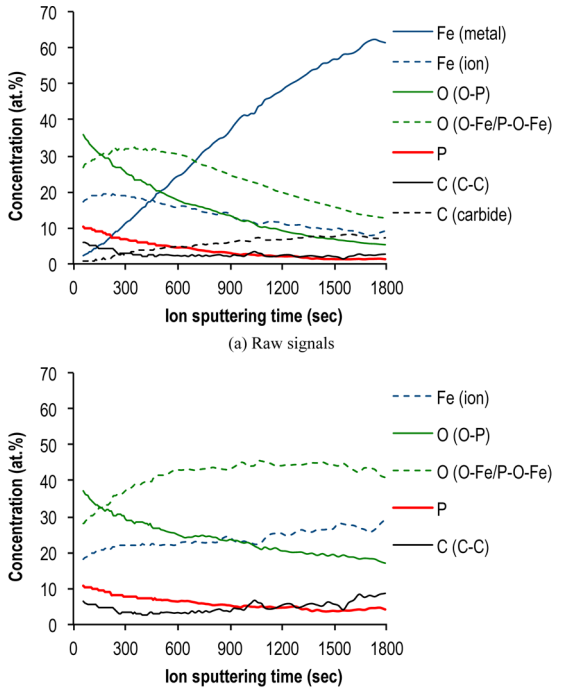

(a) Raw signals

(b) Re-normalized after removing Fe (metal) and C (carbide) from the exposed substrate

Figure 8. XPS composition-depth profile of the tribofilm on the cast iron surface lubricated by GTL 4 + $[P_{8888}][DEHP]$.

indicate two possibilities: (1) phosphates gradually decrease while iron oxides increase inside the tribofilm from the top surface to the interface with the substrate, and (2) preferential sputtering removes phosphates faster than oxides.

The carefully designed group of five ILs with identical phosphate anions but different phosphonium cations allowed a systematic study of the effects of cation alkyl chain length and symmetry on critical physicochemical and tribological properties, which provide fundamental insights for future cation design in developing the promising phosphonium-phosphate ILs as lubricant additives. A new U.S. patent application[25] has recently been filed for the phosphonium-organophosphate ILs containing symmetric cations. Results suggest oil-soluble phosphonium-phosphate ILs as potentially candidate lubricant additives in friction and wear control, which may help allow the use of lower viscosity engine and industrial oils to improve machinery efficiency and durability.

4. CONCLUSIONS

This study systematically investigated the effects of cation alkyl chain length and symmetry for quaternary phosphonium-organophosphate ILs to correlate between the cation structure and critical physicochemical and lubricating properties. Five ILs containing an identical anion but different cations, $[P_{8888}][DEHP]$, $[P_{66614}][DEHP]$, $[P_{44414}][DEHP]$, $[P_{4448}][DEHP]$, and $[P_{4444}][DEHP]$, were designed, synthesized, characterized, and evaluated as antiwear additives in a GTL 4 cSt base oil. As expected, larger cations proved to be more soluble in the base oil with six carbons per alkyl chain being a critical minimum for oil miscibility in this case. Symmetry and smaller alkyl chain lengths on the cation seemed to increase density and thermal stability due to closer packing, and more planes of symmetry and/or longer alkyls served to increase IL viscosity. No corrosive attack by any IL on cast iron was observed in open-air or electrochemical tests. Both the two oil-miscible ILs $[P_{8888}][DEHP]$ and $[P_{66614}][DEHP]$ provided effective wear protection when added to the base oil at a treat rate of 1.04 wt %. Characterization results revealed a 10−200 nm thick amorphous-nanocrystalline tribofilm, consisting primarily of iron phosphates and oxides, on the worn cast iron surface lubricated by the GTL 4 + 1.04% $[P_{8888}][DEHP]$. The symmetric-cation $[P_{8888}][DEHP]$ moderately outperformed the asymmetric-cation $[P_{66614}][DEHP]$. The hypothetical explanation for this observation of symmetry allowing higher ion mobility throughout the oil warrants further investigation.

AUTHOR INFORMATION

Corresponding Author

*Phone: (865) 576-9304. E-mail: qujn@ornl.gov.

Notes

The authors declare no competing financial interest.

ACKNOWLEDGMENTS

The authors thank Dr. J. Dyck and Dr. T. Graham from Cytec Industries Inc. for providing phosphonium cation feedstocks and $[P_{4444}][DEHP]$ and measuring the purity of $[P_{4444}][DEHP]$ and $[P_{66614}][DEHP]$. Also, we thank Dr. H.H. Elsentriecy, Dr. Y. Zhou, and D.W. Coffey from ORNL for electrochemical corrosion tests, TGA measurements, and TEM sample preparation, respectively. This research was sponsored by the Vehicle Technologies Office, Office of Energy Efficiency and Renewable Energy, US Department of Energy (DOE). Electron microscopy characterization was performed at ORNL's Center for Nanophase Materials Sciences (CNMS), sponsored by the Scientific User Facilities Division, Office of DOE-BES. W.C.B. was supported by the DOE Science Undergraduate Laboratory Internships program (SULI) and the Higher Education Research Experience (HERE) program.

REFERENCES

(1) Holmberg, K.; Andersson, P.; Erdemir, A. Global Energy Consumption Due to Friction in Passenger Cars. *Tribol. Int.* **2012**, *47*, 221−234.

(2) Ye, C.; Liu, W.; Chen, Y.; Yu, L. Room-Temperature Ionic Liquids: a Novel Versatile Lubricant. *Chem. Commun.* **2001**, 2244−2245.

(3) Mu, Z.; Liu, W.; Zhang, S.; Zhou, F. Functional Room-Temperature Ionic Liquids as Lubricants for an Aluminum-on-Steel System. *Chem. Lett.* **2004**, *33*, 524−525.

(4) Phillips, B. S.; Zabinski, J. S. Ionic Liquid Lubrication Effects on Ceramics in a Water Environment. *Tribol. Lett.* **2004**, *17*, 533−541.

(5) González, R.; Hernández Battez, A.; Blanco, D.; Viesca, J. L.; Fernández-González, A. Lubrication of TiN, CrN and DLC PVD Coatings with 1-butyl-1-methylpyrrolidinium tris(pentafluoroethyl)-trifluorophosphate. *Tribol. Lett.* **2010**, *40*, 269−277.

(6) Liu, W.; Ye, C.; Gong, Q.; Wang, H.; Wang, P. Tribological Performance of Room-temperature Ionic Liquids as Lubricant. *Tribol. Lett.* **2002**, *13*, 81−85.

(7) Chen, Y. M.; Zeng, Z. X.; Yang, S. R.; Zhang, J. Y. The Tribological Performance of BCN Films Under Ionic Liquids Lubrication. *Diamond Relat. Mater.* **2009**, *18*, 20−26.

(8) Qu, J.; Truhan, J. J.; Dai, S.; Luo, H. M.; Blau, P. J. *Lubricants or Lubricant Additives Composed of Ionic Liquids Containing Ammonium Cations*, U.S. Patent 7754664.

(9) Qu, J.; Truhan, J. J.; Dai, S.; Luo, H. M.; Blau, P. J. Ionic Liquids with Ammonium Cations as Lubricants or Additives. *Tribol. Lett.* **2006**, *22*, 207−214.

(10) Jiménez, A. E.; Bermudez, M. D.; Iglesias, P.; Carrion, F. J.; Martinez-Nicolas, G. 1-N-Alkyl-3-Methylimidazolium Ionic Liquids as Neat Lubricants and Lubricant Additives in Steel-Aluminium Contacts. *Wear* **2006**, *260*, 766−782.

(11) Jiménez, A. E.; Bermudez, M. D. Imidazolium Ionic Liquids as Additives of the Synthetic Ester Propylene Glycol Dioleate in Aluminium−Steel Lubrication. *Wear* **2008**, *265*, 787−798.

(12) Qu, J.; Blau, P. J.; Dai, S.; Luo, H. M.; Meyer, H. M., III. Ionic Liquids as Novel Lubricants and Additives for Diesel Engine Applications. *Tribol. Lett.* **2009**, *35*, 181−189.

(13) Mistry, K.; Fox, M. F.; Priest, M. J. Lubrication of an Electroplated Nickel Matrix Silicon Carbide Coated Eutectic Aluminium-Silicon Alloy Automotive CylinderBore with an Ionic Liquid as a Lubricant Additive. *Eng. Tribol.* **2009**, *223*, 563−569.

(14) Lu, R. G.; Nanao, H.; Kobayashi, K.; Kubo, T.; Mori, S. J. Effect of Lubricant Additives on Tribochemical Decomposition of Hydrocarbon Oil on Nascent Steel Surfaces. *J. Jpn. Petrol. Inst.* **2010**, *53*, 55−60.

(15) Schneider, A.; Brenner, J.; Tomastik, C.; Franek, F. Capacity of Selected Ionic Liquids as Alternative EP/AW Additive. *Lubr. Sci.* **2010**, *22*, 215−223.

(16) Yao, M. H.; Liang, Y. M.; Xia, Y. Q.; Zhou, F. Bis-imidazolium Ionic Liquids as the High Performance Anti-wear Additives in Polyethylene Glycol for Steel-Steel Contacts. *ACS Appl. Mater. Interfaces* **2009**, *1*, 467−471.

(17) Cai, M. R.; Liang, Y. M.; Yao, M. H.; Xia, Y. Q.; Zhou, F.; Liu, W. M. Imidazolium Ionic Liquids as Antiwear and Antioxidant Additive in poly(ethylene glycol) for Steel/steel Contacts. *ACS Appl. Mater. Interfaces* **2010**, *2*, 870−876.

(18) Qu, J.; Bansal, D. G.; Yu, Bo; Howe, J. Y.; Luo, H.; Dai, S.; Li, H.; Blau, P. J.; Bunting, B. G.; Mordukhovich, G.; Smolenski, D. J. Antiwear Performance and Mechanism of an Oil-miscible Ionic Liquid as a Lubricant Additive. *ACS Appl. Mater. Interfaces* **2012**, *4*, 997−1002.

(19) Yu, B.; Bansal, D. G.; Qu, J.; Sun, X.; Luo, H.; Dai, S.; Blau, P. J.; Bunting, B. G.; Mordukhovich, G.; Smolenski, D. J. Oil-Miscible and Non-Corrosive Ionic Liquids as Candidate Lubricant Additives. *Wear* **2012**, *289*, 58−64.

(20) Qu, J.; Luo, H.; Chi, M. C.; Ma, C.; Blau, P. J.; Dai, S.; Viola, M. B. Comparison of an Oil-Miscible Ionic Liquid and ZDDP as a Lubricant Anti-wear Additive. *Tribol. Int.* **2014**, *71*, 88−97.

(21) Somers, A. E.; Khemchandani, B.; Howlett, P. C.; Sun, J.; MacFarlane, D. R.; Forsyth, M. Ionic Liquids as Antiwear Additives in Base Oils: Influence of Structure on Miscibility and Antiwear Performance for Steel on Aluminum. *ACS Appl. Mater. Interfaces* **2013**, *5*, 11544−11553.

(22) Otero, I.; Lopez, E. R.; Reichelt, M.; Villanueva, M.; Salgado, J.; Fernańdez, J. onic Liquids Based on Phosphonium Cations As Neat Lubricants or Lubricant Additives for a Steel/Steel Contact. *ACS Appl. Mater. Interfaces* **2014**, *6*, 13115−13128.

(23) Qu, J.; Luo, H.; Zhou, Y.; Dyck, J.; Graham, T. Ionic Liquids Containing Quaternary Phosphonium Cations and Carboxylate Anions, and Their Use as Lubricant Additives. U.S. Patent Application 14/444,029, Jul. 28, 2014.

(24) Zhou, Y.; Dyck, J.; Graham, T.; Luo, H.; Leonard, D. N.; Qu, J. Ionic Liquids Composed of Phosphonium Cations and Organophosphate, Carboxylate, and Sulfonate as Lubricant Antiwear Additives. *Langmuir* **2014**, *30*, 13301−13311.

(25) Qu, J.; Luo, H. Ionic Liquids Containing Symmetric Quaternary Phosphonium Cations and Phosphorus-Containing Anions, and Their Use as Lubricant Additives. U.S. Patent Application 14/184,754, Feb. 20, 2014.

(26) Liang, C.-H.; Ho, W.-Y.; Yeh, L.-H.; Cheng, Y.-S.; Chou, T.-H. Effects of 1-Hexadecyl-3-methylimidazolium Ionic Liquids on the Physicochemical Characteristics and Cytotoxicity of Phosphatidylcholine Vesicles. *Colloids Surf., A* **2013**, *436*, 1083−1091.

(27) Odiowei, S.; Roylance, B. J.; Xie, L. Z. An Experimental Study of Initial Scuffing and Recovery in Sliding Wear Using a Four-Ball Machine. *Wear* **1987**, *117*, 267−287.

(28) Qu, J.; Truhan, J. J.; Blau, P. J. Detecting the Onset of Localized Scuffing with the Pin-on-Twin Fuel-Lubricated Test for Heavy Duty Diesel Fuel Injectors. *Int. J. Engine Res.* **2005**, *6*, 1−9.

(29) Qu, J.; Chi, M.; Meyer, H. M., III; Blau, P. J.; Dai, S.; Luo, H. Nanostructure and Composition of Tribo-Boundary Films Formed in Ionic Liquid Lubrication. *Tribol. Lett.* **2011**, *43*, 205−211.